

## Bloch theorem on the Bloch sphere

T. Lu,<sup>2</sup> X. Miao,<sup>1</sup> and H. Metcalf<sup>1</sup>

<sup>1</sup>Physics and Astronomy Department, Stony Brook University, Stony Brook, New York 11790-3800, USA

<sup>2</sup>Applied Math and Statistics Department, Stony Brook University, Stony Brook, New York 11790-3600, USA

(Received 22 February 2005; published 27 June 2005)

Motivated by the production of strong optical forces on atoms, we have done numerical studies of adiabatic rapid passage in light that is both frequency and amplitude modulated in the form of chirped pulses, and we found unanticipated regularities. We have quantified these regularities in terms of a periodic Hamiltonian, and obtained a result similar to the Bloch theorem, but in the time domain. This led to further numerical studies and a quantitative description of the behavior of an atom under multiply repetitive sweeps.

DOI: 10.1103/PhysRevA.71.061405

PACS number(s): 32.80.Pj, 42.50.Vk

The coherent exchange of momentum between light and atoms can produce forces much larger than the ordinary radiative force  $F_{rad} \equiv \hbar k \gamma / 2$  that has been used for most laser cooling experiments since the early 1980s. Here  $\lambda \equiv 2\pi/k$  is the wavelength of the transition to an excited state of lifetime  $\tau \equiv 1/\gamma$ . The large value of the force arises because such an exchange can be driven at a rate much faster than  $\gamma$ . The case of light with two well-defined frequencies that produces the bichromatic force has been considered as far back as 1988 [1], observed in 1989 [2], demonstrated again in 1997 [3], and more thoroughly investigated since then [4,5] and references therein. In this paper we expand on our earlier studies [6] of strong optical forces using frequency-swept light, whose spectrum is much more complicated.

Adiabatic rapid passage is a long-studied method of inverting the population of a two-level system that was well known since the early days of magnetic resonance. Its exploitation for producing large optical forces requires repeated frequency sweeps with differently directed light beams that coherently exchange momentum between the beams, imparting the difference to the atoms. The most common case is counterpropagating beams where  $2\hbar k$  is exchanged in each cycle. When these cycles are repeated at rate  $\omega_m \gg \gamma$  the force is  $F_{ARP} = \hbar k \omega_m / \pi \gg F_{rad}$ .

Perhaps the easiest way to envision the process is in a dressed atom view of the energies of a two-level system. The energies of a pair of coupled levels in this picture are

$$E_{\pm} = \pm (\hbar/2) \sqrt{\delta^2 + \Omega^2}, \quad (1)$$

where  $\delta \equiv \omega_{\ell} - \omega_a$  is the detuning of the light at frequency  $\omega_{\ell}$  from atomic resonance at  $\omega_a$ , and  $\Omega \equiv e \langle g | \vec{\mathcal{E}} \cdot \vec{r} | e \rangle / \hbar$  is the Rabi frequency that characterizes the on-resonance, electric dipole interaction between the light and atoms.

An important aspect of the dressed atom picture for the present concern is the energy ordering of the eigenstates. In the low-intensity domain (characterized by  $\Omega < \delta$ ) the upper eigenstate approaches the ground state  $|g\rangle$  and the lower one approaches the excited state  $|e\rangle$  for the case of  $\delta > 0$  but the reverse is true for  $\delta < 0$ . A plot of Eq. (1) is shown in Fig. 1 showing these limits near the  $\Omega = 0$  plane, and also that these bare ground and excited states  $|g\rangle$  and  $|e\rangle$  are otherwise

mixed on two eigenenergy sheets away from the low intensity limit (see Ref. [7]).

The process of adiabatic rapid passage (ARP) in this view involves a synchronized sweep of both the amplitude and frequency of the light so that the state of the system follows a trajectory similar to that of the heavy line in Fig. 1 ( $\delta_0$  is the amplitude of the frequency sweep). As long as travel along this trajectory is slow enough to avoid a nonadiabatic transition to the complementary eigenenergy sheet, the population will be completely inverted. Motion on the low energy sheet also can be adiabatic. For optical transitions there is always decay of  $|e\rangle$  by spontaneous emission at a rate  $\gamma$ , and the ‘‘R’’ in ARP is to require that the sweep rate  $\omega_m$  satisfies  $\omega_m \gg \gamma$ .

Production of a strong optical force on atoms requires very many such repetitive sweeps, each exchanging momentum  $\hbar k$ , and so the probability for nonadiabatic transitions must be very small for this to succeed. The probability of such unwanted transitions can be found from the small fraction of population on the ‘‘wrong’’ energy sheet after each sweep where  $\Omega = 0$  so the eigenstates are exactly the bare states. During the course of very many such sweeps, sponta-

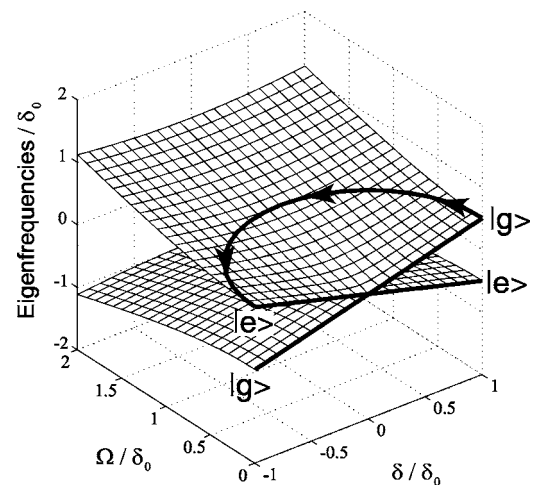


FIG. 1. A plot of Eq. (1). The dressed states comprise two separated sheets except at the conical intersection at the origin. The upper (lower) state is ground at  $\Omega = 0$  for  $\delta > 0$  ( $\delta < 0$ ). The indicated path is a possible trajectory for ARP.

neous emission is likely to occur, and this resets the wave function to  $|g\rangle$  at a random time relative to the sweep clock. We anticipate that its effects can be ameliorated by syncopation of the sweeps, just as in the case of the bichromatic force [4,5].

A more common view of ARP is couched in the language of the Bloch vector  $\vec{R}$  moving on the Bloch sphere under the influence of a light field whose frequency and intensity are both modulated at rate  $\omega_m$ . The vertical axis ( $z$ ) of the sphere is the population difference term and the horizontal axes are related to the relative phase of the atomic superposition, determined by the mixing of the atomic states by the optical field (see Refs. [8,9]). The equation of motion is

$$\frac{d\vec{R}}{dt} = \vec{\Omega}(t) \times \vec{R}, \quad (2)$$

where  $\vec{\Omega}(t)$  is an artificial ‘‘torque’’ vector having components  $[\vec{\Omega}(t), 0, \delta(t)]$ . Its component in the equatorial plane depends on phase, but may be chosen to be along the  $x$  axis without loss of generality. ARP consists of sweeping the optical frequency from one side of resonance to the other, so that the torque vector starts and ends nearly along the polar axis, but sweeps through the equatorial plane at  $\delta=0$  [10]. The process is more efficient if the start and end points of  $\vec{\Omega}(t)$  are closer to the polar axis of the Bloch sphere, suggesting the light intensity should be modulated synchronously to be minimum at the extrema of the frequency sweep. This notion leads to pulsing of the light and thus the trajectory of Fig. 1.

If the time dependence of the intensity is described by  $\Omega(t) = \Omega_0 \sin \omega_m t$  and the frequency sweep is characterized by  $\delta(t) = \delta_0 \cos \omega_m t$ , then the special case of  $\Omega_0 = \delta_0$  has been studied in some detail [11]. The consequence of this special case is that  $\vec{\Omega}$  satisfies

$$\frac{d\vec{\Omega}}{dt} = \vec{A} \times \vec{\Omega}, \quad (3)$$

where  $\vec{A}$  is an artificial constant vector so that  $|\vec{\Omega}|$  is constant. The Landau-Zener (LZ) formula gives the probability of the nonadiabatic transition  $P_{NA} = e^{-\pi\eta/2} \rightarrow 0$  because  $d|\vec{\Omega}|/dt = 0$  [ $\eta \equiv |\vec{\Omega}|^2 / (d|\vec{\Omega}|/dt)$ ]. LZ is asymptotically correct for large  $\delta_0$  ( $\delta_0 \gg \omega_m$ ), but the variations of  $P_{NA}$  as obtained in Ref. [11] are lost. These authors are concerned with nonadiabatic transitions between the energy sheets of Fig. 1 as are we, but their calculations are limited to the case of Eq. (3).

Still, their analytic results, that are valid for all values of  $|\vec{A}|/|\Omega_0|$  (hence their title), provide a series of values of  $|\vec{A}|/|\Omega_0|$  where the probability of such nonadiabatic transitions is vanishingly small. Since we are concerned with a large optical force resulting from very many adiabatic sweeps, these solutions are of great interest.

Our first step was numerical integration of Eq. (2) under the condition of Ref. [11], assuming the atom starts at the ground state, i.e., the initial Bloch vector  $\vec{R}$  is at the south pole. We integrate for a single sweep (half cycle) and calcu-

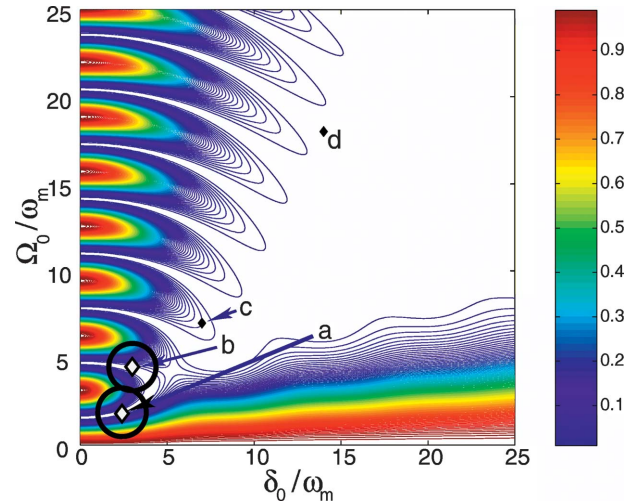


FIG. 2. (Color) A contour plot of the numerical values of  $\rho_{gg}$  vs  $\delta_0$  and  $\Omega_0$  after one sweep. The diagonal of this plot reproduces the results of Ref. [11], but our coordinate is the reciprocal of their ‘‘rapidity’’ parameter. The large open areas toward the upper right represent regions where  $\rho_{gg} < .01$  so the probability of nonadiabatic transitions is negligibly small. Each contour line is a step of 0.01 so the point (c) is at  $\rho_{gg} = 0.02$ . Interest lies in those special areas that are close to the origin where  $\rho_{gg}$  is still tiny. The pathway along the vertical axis,  $\delta_0 = 0$ , that is punctuated by narrow white regions represents pulses of area  $n\pi$  that also produce inversion ( $n = \text{odd integer}$ ). The indicated points represent  $(\delta_0/\omega_m, \Omega_0/\omega_m) = (a) -(2.4, 1.8)$ , (b)  $-(3, 4.4)$ , (c)  $-(7, 7)$ , and (d)  $-(14, 18)$ .

late the excited state component of the population. Ideally,  $\vec{R}$  ends near the north pole and the population is nearly inverted, thus  $\hbar k$  is absorbed from the light field. The remaining ground state population at the end of the sweep,  $\rho_{gg}$ , or in terms of the parameter  $w$  of Ref. [9],  $\rho_{gg} = (1-w)/2$ , gives the nonadiabatic transition rate of the process. For the case of  $|\vec{\Omega}|$  constant [Eq. (3)], we reproduce the results of Ref. [11].

Our numerical calculation is not restricted by Eq. (3) and so in Fig. 2 we plot  $\rho_{gg}$  for various values of  $\delta_0$  and  $\Omega_0$ , both in units of  $\omega_m$ . The diagonal of Fig. 2 corresponds to the semicircular paths in Fig. 1, but other points correspond to various elliptical trajectories.

Now we consider a second pulse, i.e., the second half cycle. Then  $\vec{R}$  will be inverted back near the south pole. Note that  $\vec{R}$  lying near the south pole after two sweeps doesn’t guarantee the population inversion after one sweep, although the converse is true. A strong force requires not only the population inversion but also that the two pulses have different  $\vec{k}$  vectors, but the evolution of  $\vec{R}$  does not depend on the  $\vec{k}$  vectors.

We also have begun analytical calculations in the instantaneous eigenspace of the Hamiltonian and our preliminary approximate results for the nonadiabatic transition probability agree very well with Fig. 2.

The sweep of the laser parameters produces an evolution of the Bloch vector  $\vec{R}$ , and each cycle of two pulses lasts for  $T = 2\pi/\omega_m$ . We consider a cycle as an operator that transforms  $\vec{R}$  according to

$$\vec{R}(t) = U(t)\vec{R}(0), \quad (4)$$

where  $U(t)$  is determined by the history of  $\vec{\Omega}$  from  $t=0$  to  $t$ . For simplicity we assign  $t=0$  to the start of the first sweep. The operator  $U(t)$  must leave  $\vec{R}$  on the surface of the Bloch sphere. In the appendix we show that  $U(t)$  is in fact a rotation of  $\vec{R}$  and we choose to view it as a rotation of the sphere instead. This view allows us to treat all cycles equally since the rotation of the sphere doesn't depend on  $\vec{R}$ . Although  $U(t)$  may turn the sphere in a very complicated way, certainly nearly inverting it so that  $\vec{R}$  passes near the north pole midway through a cycle (between the two sweeps), we are presently concerned only with the result at the end of each cycle and so consider only  $\vec{R}(jT)$ , where  $j$  is an integer.

Our discussion begins with  $\vec{R}(0)=(0,0,-1)$  so that the first cycle transforms it to  $\vec{R}(T)$ , displaced from the south pole through some angle  $\beta$ . For a plane containing  $\vec{R}(T)$  and the south pole,  $\vec{R}(T)=[U(t=T)\vec{R}(0)]$  could be the result of a rotation by  $\beta$  about an axis *perpendicular* to this plane, a rotation by  $\pi/2$  about an axis tilted at  $\beta/2$  to the polar axis *in* this plane, or through a set of angles and related axes between these extremes. In general, the axis is not in this plane so it requires two angles to specify its orientation.

The two angles required to specify the axis are the spherical coordinates  $\theta_a$  and  $\phi_a$ , and  $\alpha$  specifies the rotation. All three of these are dependent on the details of the laser parameter sweep  $\vec{\Omega}(t)$ . What is important is that the angle and the axis are the same for every cycle since  $U(T)$  is a rotation, and so the set of  $j$  points marking the values of  $\vec{R}(jT)$  on the sphere lie on a circle that passes through the south pole for our chosen initial condition  $\vec{R}(0)=(0,0,-1)$ , i.e.,  $\vec{R}(0)$  on the south pole.

The center of this circle of points  $\vec{R}(jT)$  lies on the axis of rotation, tilted by an angle  $\theta_a$  from the polar axis. For the case where the laser parameters are nearly ideal so that all  $\vec{R}(jT)$ 's are near the south pole, the radius of this circle  $r_0 \ll 1$  ( $|\vec{R}|=1$ ). Thus it is most easily visualized when viewing the Bloch sphere from below, along its polar axis. The circular locus of values of  $\vec{R}(jT)$  has points separated by  $\alpha r_0$  with its center at  $(\theta_a, \phi_a)$ . If  $\alpha$  is a rational multiple of  $2\pi$  the points cyclically overlap, and if not, they form a discontinuous circle. Figure 3 shows a plot of our numerical results for a few particular cases.

Since  $U(T)$  is a rotation (see appendix), it can be written as  $U=e^{i\alpha\hat{J}\cdot\hat{u}/\hbar}$ , where  $\hat{u}$  is a unit vector along the rotation axis determined by  $\theta_a$  and  $\phi_a$ , and  $\hat{J}$  is the spin-1 vector operator. One can also apply the Floquet theorem here because of the periodicity of the linear equations being considered. So there exist solutions that only change by a phase factor after each period  $T$ , which are the so-called Floquet states. For these states,  $R(jT)$  can be written as a phase factor  $\langle U(jT) \rangle$ , which is the expectation value of  $U(jT)$  at  $R(0)$ , times the original  $R(0)$  for every  $j$ , and this is mathematically analogous to the Bloch theorem.

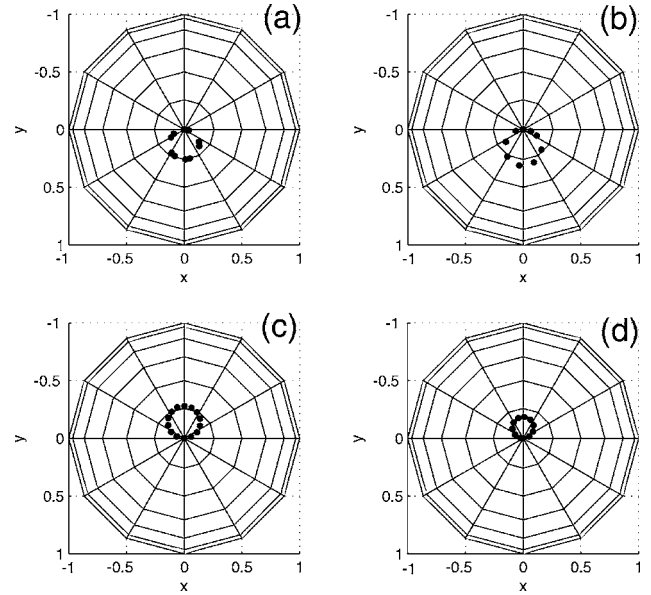


FIG. 3. Plots showing the calculated values of  $\vec{R}(jT)$  on the Bloch sphere as viewed from the south pole. Each set of points lies on a circle whose radius and center depend on the sweep parameters. These parameters are the same as those for parts (a) through (d) of Fig. 2. The points appear to be not evenly spaced [e.g., part (a)] because the rotation angle is large and more than one full rotation is shown.

At the end of every cycle (pair of pulses),  $\vec{R}$  is to be found somewhere on a small circle near the south pole as shown in Fig. 3. Since the trajectory  $\vec{R}(t)$  of all the  $\vec{R}(jT)$ 's during the pulse can also be represented by the rotation of the Bloch sphere, that circle is preserved throughout the cycle. It rotates as it moves, but cannot be distorted since the sphere itself that is rotating. Thus the paths swept out by the tip of all the  $\vec{R}$ 's remain within a band of width equal to the diameter of that circle  $2r_0$ . A few such trajectories are plotted in Fig. 4.

Figure 5 can be used to calculate how  $\rho_{ee}$  varies from one cycle to the next. Figure 5(a), enlarged for clarity, shows a view from the south pole of the circle defined by the  $\vec{R}(jT)$ 's. The large dot on the left marked "S" is the starting point at the south pole, and "E" marks the  $n$ th point. The distance  $SE^2=r^2=2r_0^2(1-\cos n\alpha)$ .

Figure 5(b) is a side view of the entire Bloch sphere showing the south pole at S and the north pole at N. The plane containing the circle in Fig. 5(a) is represented by the line SE. Since  $BS/SE=SE/2$ ,  $\rho_{ee}=BS/2=r_0^2(1-\cos n\alpha)/2$ . Since the time for each step is  $T=2\pi/\omega_m$ , we have  $\rho_{ee}(j)=r_0^2[1-\cos(\alpha\omega_m jT/2\pi)]/2$ . Hence  $\langle \rho_{ee} \rangle_j=r_0^2/2$ .

ARP has the capability of transferring up to  $2\hbar k$  of momentum between a light field and an atom in a very short time, but the production of a large force requires that the process be stable and robust under many repetitions ( $\sim 10^4$ ). Our investigations reported here delineate the surprisingly large region of parameter space where this is indeed the case.

The authors acknowledge financial support from the ONR and the NSF.

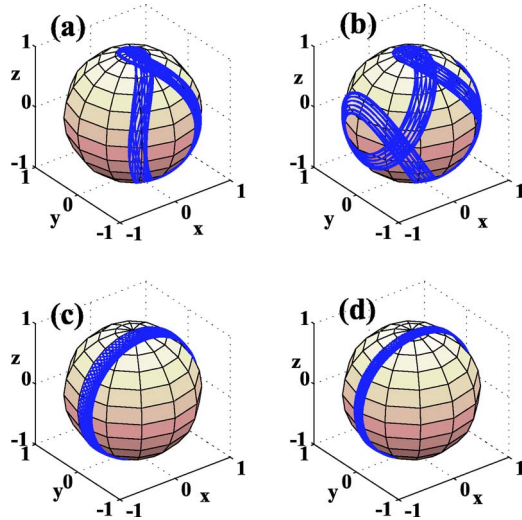


FIG. 4. A set of trajectories of  $\vec{R}$  on the Bloch sphere using the same laser parameters as in Figs. 2 and 3. The trajectories are confined to bands whose nearly constant width is essentially the same as the diameter of the circles of Fig. 3.

#### APPENDIX

We show that a chirped light pulse described by  $\vec{\Omega}(t)$  acts on the Bloch vector as a rotation of the Bloch sphere. To do this we first construct an operator  $U(t)$  that satisfies Eq. (4). Then we show that it is indeed a rotation because it is orthogonal, unitary, and conserves parity.

The existence is without question because Eq. (2) can be integrated directly. For example, for each of the three possible initial conditions,  $\vec{R}_j(0) = (1, 0, 0), (0, 1, 0), (0, 0, 1)$ ,  $j = 1-3$ , their transformations to  $\vec{R}_j(t)$  can be calculated directly, even as  $\vec{\Omega}(t)$  varies over time, because it is continuous, finite, and differentiable. Since Eq. (4) is linear,  $U(t)$  can be calculated for any  $\vec{R}(0)$ , and in fact, it is the  $3 \times 3$  matrix

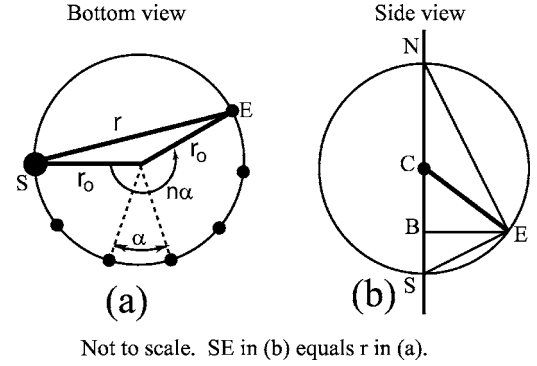


FIG. 5. (a) shows the circle of the  $\vec{R}(jT)$ 's on a view of the Bloch sphere from the south pole (marked "S"). Here  $SE^2 = r^2 = 2r_0^2(1 - \cos n\alpha)$ ; (b) is a side view: note that the circle of (a) projects onto the line SE.

$U(t) = [\vec{R}_1(t), \vec{R}_2(t), \vec{R}_3(t)]$ , where the  $\vec{R}_j(t)$ 's are the columns.

Orthogonality and unitarity are straightforward. The initial dot products satisfy  $\vec{R}_i(0) \cdot \vec{R}_j(0) = \delta_{ij}$  and Eq. (2) shows that the time derivatives of the dot products are

$$\begin{aligned} \frac{d}{dt}[\vec{R}_i(t) \cdot \vec{R}_j(t)] &= [\vec{\Omega} \times \vec{R}_i(t)] \cdot \vec{R}_j(t) + \vec{R}_i(t) \cdot [\vec{\Omega} \times \vec{R}_j(t)] \\ &= \vec{\Omega} \cdot [\vec{R}_i(t) \times \vec{R}_j(t) + \vec{R}_j(t) \times \vec{R}_i(t)]. \quad (\text{A1}) \end{aligned}$$

For  $i=j$  the dot product on the top line is  $|\vec{R}|^2$ . Since each cross product in the last line of Eq. (A1) is zero,  $|\vec{R}|$  does not change so  $U(t)$  is unitary. For the case  $i \neq j$ , the cross-product terms are equal and opposite so they cancel, and again the dot product on the first line is constant. Thus the (nonzero) components  $\vec{R}_i(t)$  and  $\vec{R}_j(t)$  remain orthogonal for all  $t$  so  $U(t)$  is orthogonal. Finally, parity conservation is assured because  $U(t)$  can be written as a set of infinitesimal rotations, none of which can change  $\det\{U(t=0)\}$  from  $+1$  to  $-1$ .

- [1] V. Voitsekhovich *et al.*, Zh. Tekh. Fiz. **58**, 1174 (1988) [Sov. Phys. Tech. Phys. **33**, 690 (1988)].  
 [2] V. Voitsekhovich *et al.*, Pis'ma Zh. Eksp. Teor. Fiz. **49**, 138 (1989) [JETP Lett. **49**, 161 (1989)].  
 [3] J. Söding *et al.*, Phys. Rev. Lett. **78**, 1420 (1997).  
 [4] M. Partlow *et al.*, Phys. Rev. Lett. **93**, 213004 (2004).  
 [5] L. Yatsenko and H. Metcalf, Phys. Rev. A **70**, 063402 (2004).  
 [6] M. Cashen *et al.*, J. Opt. B: Quantum Semiclassical Opt. **4**, 75

- (2002).  
 [7] L. P. Yatsenko *et al.*, Phys. Rev. A **65**, 043407 (2002).  
 [8] R. Feynman *et al.*, J. Appl. Phys. **28**, 49 (1957).  
 [9] L. Allen and J. Eberly, *Optical Resonance and Two-Level Atoms* (Dover, New York, 1987).  
 [10] H. Metcalf and P. van der Straten, *Laser Cooling and Trapping* (Springer, Berlin, 1999).  
 [11] D. Sawicki and J. H. Eberly, Opt. Express **4**, 217 (1999).